In silico analysis and *in planta* production of recombinant *ccl21/IL1β* protein and characterization of its *in vitro* anti-tumor and immunogenic activity

Hasan Marashi [a]-Maria Beihaghi[ab] * Samad Khaksar[b]

a College of Agriculture, Ferdowsi University of Mashhad, Mashhad, Iran
b School of Science and Technology, The University of Georgia, Tbilisi, Georgia
Email: marashi@um.ac.ir ORCID num: https://orcid.org/0000-0002-3545-7487
Emai:maria_beihaghi@yahoo.com ORCID num:https://orcid.org/0000-0001-8356-3818

Abstract

CCL21 has an essential role in anti-tumor immune activity. Epitopes of IL1β have adjuvant activity without causing inflammatory responses. CCR7 and its ligands play a vital role in the immune balance; specifically, in transport of T lymphocytes and antigen-presenting cells such as dendritic cells to the lymph nodes. This study aimed to produce epitopes of CCL21 and IL1β as a recombinant protein and characterize it's *in vitro* anti-tumor and immunogenic activity. A codon-optimized *ccl21/IL1β* gene was designed and synthesized from human genes. Stability and binding affinity of CCL21/IL1β protein and CCR7 receptor were examined through *in silico* analyses. The construct was introduced into *N. tabacum* to produce this recombinant protein and the structure and function of CCL21/IL1β were examined. Purified protein from transgenic leaves generated a strong signal in SDS PAGE and western blotting assays. FTIR measurement and MALDI-TOF/TOF mass spectrography showed that *ccl21/IL-1β* was correctly expressed in tobacco plants. Potential activity of purified CCL21/IL1β in stimulating the proliferation and migration of MCF7CCR7+ cancer cell line was investigated using the wound healing method. The results demonstrated a decrease in survival rate and metastasization of cancer cells in the presence of CCL21/IL1β, and IC_{50} of CCL21 on MCF7 cells was less than that of non-recombinant protein. Agarose assay on PBMCsCCR7+ showed that CCL21/IL1β has biological activity and there is a distinguishable difference between chemokinetic (CCL21) and chemotactic (FBS) movements. Overall, the results suggest that CCL21/IL1β could be considered an effective adjuvant in future *in vivo* and clinical tests.

Keywords: CCL21/IL1β, Coronavirus disease, molecular dynamics simulation, FTIR, Scratch assay, Chemotaxis assay.

Introduction

Cytokines are small proteins crucial to the cell signaling of the immune system, affecting the function and behavior of the cells around them. They include lymphokines, interferons, tumor necrosis factors, chemokines, and interleukins[1]. Chemokines activate inflammatory pathways and direct leukocyte migration [2, 3]. CC chemokine ligand 21 (CCL21) is a chemokine without inflammatory responses, which attracts normal immune cells and metastasizing tumor cells to lymph nodes by activating the CCR7 receptor [4]. CCR7 is expressed on many cancer tumor cells and naïve T-cells [5]. Moreover, CCL21 is a recognized attractant for CCR7-positive (CCR7+) cells [6]. Therefore, CCL21/CCR7 has essential roles in lymphatic cancer metastasis, immune cell and lymph-node homing, peripheral tolerance, development, and function of T regulatory cells in such diseases as HIV and COVID-19 [5], lymphoid neogenesis [7, 8], and in secondary lymphoid organs. Activation of T-cells is facilitated by CCL21 through recruitment and co-localization of naïve lymphocytes and antigen-induced dendritic cells (DC) [3, 9, 10]. Accordingly, CCL21 is a base for cancer immunotherapy since it can chemoattract T-lymphocytes and DCs [11]. DCs take

up tumor antigens and migrate to T-cell zones of lymphoid organs for specific anti-tumor T-cell activity [7, 12]. Examples of CCR7+ human breast cancer cell lines are MCF7 and MDA-MB232 [13]. In addition to its anti-tumor activity, CCL21 is also effective in treating AIDS. HIV attaches to chemokine receptors such as CCR7 on the surface of CD4+ T-cells and kills immune cells. However, studies have shown that CCL21 is a chemokine that can occupy CCR7 receptors on the surface of CD4+ T-cells and prevent HIV attachment [14].

Interleukin-1 beta (IL-1β) is a potent inflammatory cytokine protein encoded by the *IL1β* gene in humans. IL-1β is also involved in various cellular activities such as activation of neutrophils, B-cells and T-cells, production of cytokines and antibodies, proliferation of fibroblasts, and collagen production [15]. The VQGEESNDK amino acid sequence is a part of IL-Iβ that has all the adjuvant activity of the entire IL-Iβ, without the inflammation and fever response. Consequently, by inserting the VQGEESNDK sequence into the synthetic construct, the immunogenicity of protein antigens is increased [16].

Major histocompatibility complex (MHC) is a part of the genome that plays an essential role in creating an immune response to protein antigens. MHC genes produce the MHC molecules. These molecules can bind to some antigenic peptides, after which the specific complex of MHC peptide will be detectable to T-lymphocytes [17]. For example, CCL21 is a Chemokine that controls cell trafficking and is involved in numerous pathologic and inflammatory conditions, and it is endocytosed with its receptor (CCR7) via both MHC class I and II processing pathways to induce CD8+ and CD4+ T-cell responses [18].

The use of plants as bioreactors for manufacturing recombinant proteins, known as molecular farming, has captured great interest among researchers over the past two decades[19]. Tobacco (*Nicotiana tabacum* L.) serves as one of the model plants used in physiological, genetic, and tissue-culture studies [20, 21]. Manipulation of the tobacco genome requires efficient transformation and regeneration techniques, making this plant an impressive bioreactor for production of recombinant proteins. Tobacco tissue culture system [20] and transformation method were optimized in the present study. Several strategies have been proposed for boosting recombinant protein expression, including the use of influential promoters, chloroplast transformation[22] [23], signal peptide codon optimization, and application of untranslated leader sequences [24]. Molecular dynamics simulation [25] is a computer simulation method used to understand the conformational changes caused by mutations in recombinant proteins [26, 27]. In addition, it can be used to analyze the highly fluctuating and complex dynamics of proteins [28].

This study aimed to investigate the expression of *ccl21/IL1β* as recombinant protein in transgenic lines. So In addition to the CCL21 sequence, this recombinant protein contains fragments of interleukin 1 beta sequences, introduced by placing epitopes related to B-lymphocytes and CTLs in the desired structure to activate T & B-lymphocytes, macrophages, and neutrophils simultaneously. It can be utilized as a potent adjuvant for treating breast cancer, especially with Her2 / neu gene expression and the Th1 immune response, which affects most drugs, alleviates the disease, and boosts immunity. Therefore, the gene construct to be expressed in tobacco plants contained a DNA fragment encoding 134 amino acids that form epitopes and which cover more than 90% of the HLA-DRB4 allele and can bind to MHCI and MHCII molecules at T-cell and CCR7 receptors. *In*

silico analysis and *in vitro* assays (such as scratch assay, MTT assay, and chemotaxis assay) were used for investigating the immunogenic function of this recombinant protein. The project was ethically approved in accordance with Code IR.MUMS.REC.1399.428.

2. Materials and Methods

2.1 *In silico* analysis

2.1.1 Construction of Expression Cassette

DNA sequences encoding human CCL21 (Accession No: O00585) and VQGEESNDK sequence of human IL-1β were designed as the principal part of the expression cassette. The designed expression cassette included Kozak consensus sequence as the plant-specific ribosome binding site (GCCACC). The CCL21 and VQGEESNDK sequences of human IL-1 beta were linked together by EAAAK sequence as beta-defensin linker. The SEKDEL signal sequence - for effectual agglomeration of the recombinant protein in the endoplasmic reticulum (ER) - and 6xHis tags were also linked by RVLAEA sequence as HIV protease linker. Recognition sites of *Bam*HI and *SacI* restriction enzymes were added to the 5' and 3' ends of the synthetic gene, respectively. AUG and UAA were also added to the construct's 5' and 3' ends as start and stop codons, respectively. The terminal part of the chimeric gene was optimized based on the codon usage pattern of tobacco according to the Codon Usage Tabulated from GenBank (CUTG) website (http://www.kazusa.or.jp/codon/) [29]

2.1.2 Prediction of solubility and stability of the recombinant protein, and its post-translational and allergenicity evaluation

Before expressing this gene construct in tobacco plants, the final gene construct was translated *in silico* into a peptide sequence. SOLpro server was used for predicting the solubility of the recombinant protein, and ProtParam online server for predicting various physicochemical parameters including amino acid composition, pI, aliphatic index (AI), instability index (II), *in vivo* and *in vitro* half-life, molecular weight (MW), and grand average of hydropathicity (GRAVY). The allergenicity of this recombinant protein was assessed by the AlgPred web server, which showed the post-translational modifications of CCL21/IL1β. NetOGlyc 4.0 Server and NetNGlyc 1.0 Server were used to identify the O-glycosylation and N-glycosylation sites of the recombinant protein, respectively; and NetPhos 3.1 Server was used to find the phosphorylation sites of the protein [29].

2.1.3 Prediction of MHC I and II binding affinities of the recombinant protein

T-cell and B-cell epitopes of the recombinant protein were identified utilizing BepiPred 2.0, BCpreds, ABCpreds, SVMTrip, and MAPPP online servers (Table 1). These bioinformatic tools have been used to predict antigenic epitopes present on T-cell and B-cell surfaces by primary histocompatibility complex class I and II molecules (MHC I, MHCII) [30]. In addition, the TAPPred server was used to verify the binding affinity of the recombinant protein toward TAP transporter. This online service is based on cascade SVM and uses the sequence and properties of amino acids.

2.1.4 Homology modeling structure using *in silico* tools

Since the three dimensional (3D) structure of the recombinant protein is not available, comparative modeling method was initially used to create the 3D structure of the recombinant protein. Comparative modeling is one of the best approaches to prediction of the 3D structure of the target protein, in which 3D structures with sequences very similar to the target sequence are used as templates. One of the best software for comparative modeling is MODELLER. The authors used Modeller 9.24 for 3D modeling of the target . Ten models were produced, and the one with the highest interaction and connectivity between the aforementioned epitopes was selected as the best model [31].

2.1.5 Molecular dynamics simulation and prediction of the stability and flexibility of the recombinant protein

After three dimensional modeling of the target recombinant protein sequence, the molecular dynamics simulation method was used to optimize the modeled structure. Molecular dynamics simulations allow researchers to observe changes in the orientation of different amino acids over time. In this method, each atom has its dynamics and motion and this causes movement in the structure of the whole protein, and one can optimize the 3D structure of the recombinant protein. Motion is the main factor in the function of biological macromolecules and this has led to development of the "dynamic relationship between activities" approach. Dynamics is the key to the stability of biological systems, including the function of enzymes, drug binding, membrane formation, and other biological processes. A change in motion causes a change in structure and thus a change in protein function. Motion can eliminate a series of interactions in the structure of the recombinant protein and thus form new interactions, which can optimize the structure of the recombinant protein. After molecular dynamics simulation, a series of analyses are used to evaluate the protein's 3D structure stability during the simulation. Molecular dynamics simulation was performed using Gromacs 2019.6 software. Input structures were prepared with ff99SB force field. The correct hydrogen bonding patterns of histidines was defined for all proteins. The surface charge of the structure was neutralized by adding chlorine ions. The protein was placed in a layer of 8 angstrom-thick TIP3P water molecules inside an octahedron box using gmx solvate software. Reduction of energy on the structures was achieved with 50,000 steps by the steepest descent method to eliminate van der Waals interactions and hydrogen bonds between water molecules and the complex. In the next step, temperature of the system was gradually increased from 0 to 310 K for 200 ps in constant volume, and then the system was equilibrated at constant pressure for 200 pc. Molecular dynamics simulations were performed at 37°C for 100 nanoseconds. Non-bonded interactions with 10-angstrom intervals were calculated by the PME method. The SHAKE method was used to restrict the hydrogen atoms involved in bonding in order to enhance computing performance. Finally, simulation data were stored at 0.4 pc intervals for analysis [28]. Two of the best methods for such analyses are root mean square deviation (RMSD) and Radius of Gyration (RG) change over time. The RMSD between the structures created during molecular dynamics simulation in the time dimension is a suitable and common standard to ensure the structural stability of the protein. Therefore, RMSD changes related to alpha carbon atoms of the protein during simulation time (100 nm) relative to the original structure were calculated and extracted. RG

is another crucial parameter used in studying changes of protein size during simulation of molecular dynamics.

2.1.6 Docking and molecular dynamics simulation of the CCL21/IL1β and CCR7 receptor

This project aimed to investigate the interaction between chemokine ligands and CCR7 receptors. The CCR7 protein is intermembrane and, therefore, to simulate the CCR7-CCL21 complex, this complex must first be located inside the plasma membrane. For this purpose, the CHARMM-GUI server was used to place the complex inside the plasma membrane. POPC phospholipid was selected to generate the lipid membrane. After placing the protein complex inside the POPC membrane according to the protocol in the CHARMM-GUI server, the desired output was selected for molecular dynamics simulation with GROMACS 2019.6 software. At this stage, after energy minimization using the steepest descent algorithm, the system was balanced in NVT conditions in a time step of 1 femtosecond for 1 nanosecond. Equilibration was then performed under NPT conditions in a time step of 2 femtoseconds for 4 nanoseconds. The Berendsen algorithm was used to keep the temperature constant at 310 K and the pressure at 1 atmosphere in NVT and NPT conditions. Also, during the equilibration process, a series of restrictions according to the protocols available on the CHARMM-GUI server was used to limit proteins, water, and phospholipid molecules. After the equilibration steps were completed, molecular dynamics simulations were performed in the production phase for 100 nanoseconds. At production stage, Nose-Hoover and Parrinello-Rahman algorithms were used to keep the temperature and the pressure constant,, respectively. The simulation time step at production stage was 2 femtoseconds, and all the limitations of solvent and soluble molecules were removed at this stage. There were 179 POPC[1] and 20443 water molecules, and 54 and 89 sodium and chlorine atoms, respectively. The simulation time was 100 nanoseconds. The cut-off values for electrostatic and van der Waals interactions were 1.2 and 1 nm, respectively. RMSD and RG were used to study the stability of the vaccine on CCR7 receptors during molecular dynamics simulation.

2.2 Stable transformation of tobacco plants with the *ccl21/IL1β* gene

Sterilized tobacco (*Nicotiana tabacum* L) seeds were germinated on MS medium with 15 g/L sucrose, solidified by 7g/L agar. The recombinant plasmid (pBI121-*ccl21/ IL1β*) was introduced into *Agrobacterium tumefaciens* strain GV3101 via the freeze and thaw method [32]. Afterward, 200µl of *Agrobacterium* suspension, containing recombinant plasmid pBI121, was transferred to 50 ml of fluid medium containing kanamycin (50 mg/l), rifampicin (50 mg/l) and gentamicin (20 mg/l), and incubated for 24 hours at 28°C. The culture was centrifuged at 5000 rpm for 5 min at 4°C, and the cells were resuspended in inoculum medium consisting of three parts MS medium (pH 5.2) and one part LB medium with 0.05 mM acetosyringone (3′, 5′-dimethoxy- 4′-hydroxy acetophenone). The suspension was placed in a dark room incubator at 28°C for half an hour. Sterile leaf disks (about 0.5 cm^2) were excised and inoculated with recombinant *Agrobacterium tumefasciens[33]*. Explants were transferred to a co-culture medium (MS with 0.2 mg/L BA and 0.1 mg/L NAA without antibiotics) and cultured for 48 hours in a dark room incubator at 25°C. After co-cultivation, the explants were transferred to the branching induction medium (MS

[1] phosphatidylcholine

203 containing 30g/L sucrose, 1 mg/L BAP, 0.1 mg/L NAA, and 300 mg/L cefotaxime and 50 mg/L
204 Kanamycin antibiotics). The selection process was continued for 14 days at 22°C on a photoperiod
205 cycle of 16 hours light and 8 hours dark (LD 16:8). The selected explants were then transferred to
206 solidified root-inducing medium (MS basal salts with 15 g/L sucrose, 0.2 mg/L NAA, and 200
207 mg/L cefotaxime). Finally, the plants were transferred to the greenhouse until the seeds of the T_1
208 generation were obtained. Growth and self-sufficiency of T_1 plants were analyzed to confirm
209 transgene stability [34].

210

211 **2.3 PCR and real-time PCR assays**

212 Genomic DNA of transgenic plants was identified by PCR analysis using two primers, *CaMV-ccl21*
213 F 5'GATGACGCACAATCCCACT 3' and *CaMV-ccl21* R 5'CCCTTTCCCTTCTTTCCA3', which
214 amplify 386 bp around the attachment region between CaMV promoter and the *ccl21* gene. In
215 addition, *nptII* F 5'CACGGTTCAACAACATCCAG3' and *nptII* R
216 5'TGAAGACCCTGACTGGGAAG3, amplifying 782 bp around the Kan R region in PBI121
217 plasmid were used. PCR was performed according to the temperature profile provided in the
218 appendix: 94ºC 1 min, 50ºC 1 min, and 72º C for 2 min for 30 cycles (Parstous kit; Cat.No
219 C101081).

220 Whole RNA was extracted from infiltrated leaf tissue (Parstous kit; Cat. No A101231), and
221 complementary DNA (cDNA) was synthesized through reverse transcription using oligo[23] primer
222 (Parstous kit; Cat.No C101131). The resulting cDNA mixtures were utilized as templates for real-
223 time PCR. Real-time PCR (BioRad) was performed in a 20 µL reaction volume containing 1 µM of
224 each primer and 10 µL of SYBR green real-time PCR master mix (Parstous kit; Cat.No C101021).
225 Real-time PCR experiments were carried out for each sample in duplicate. Forward and reverse
226 primers for real-time PCR were 5' GGGTTCAACAACTTATGC 3' and 5'
227 CTTTCCCTTCTTTCCAGT 3', respectively.

228 **2.4 Extraction and purification of Total Soluble Protein from T2 plants**

229 Total Soluble Protein (TSP) was extracted using 500 µL of 1x PBS as a biological buffer and 10 µL
230 of 100mM phenyl methane sulfonyl fluoride (PMSF) per 0.2 g leaf dry weight. The extract was
231 centrifuged at 12,000 g for 20 min at 4ºC. The extracted TSP was purified by Ni-IDA resin (Cat No:
232 A101271), and also dialysis was used to remove the imidazole contained in the protein purification
233 buffer. Purified CCL21/IL1β concentration was determined as % of Total Soluble Protein (TSP)
234 and µg/g of leaf Fresh Weight (FW).

235 **2.5 Protein dot blot assay and western blot assay**

236 Purified recombinant protein in transgenic lines was measured by standard protein dot blot assay.
237 First, 10µl of TSP from transgenic lines was dotted onto the nitrocellulose membrane, and the
238 membrane was left to dry. Next, the membrane was incubated with BSA as the blocking solution
239 for 1 hour. After incubation, the membrane was thoroughly washed three times with PBST/PBS and
240 incubated with conjugated anti-6x His tag® mouse monoclonal antibody for 1 hour at 37ºC, then
241 washed three times with PBST/PBS, and finally incubated with DAB (diaminobenzidine) substrate.

242 A small amount of commercial CCL21 antigen containing Histidine tag (1 µL) was used as the
243 positive control (Cat No: 966-6C), and 10µl of protein from the wild-type plant was used as a
244 negative control. For western blotting, 100 micrograms of TSP per sample was resolved on 12%
245 SDS-PAGE and visualized by Coomassie Brilliant Blue staining. For western blotting, the resulting
246 SDS-PAGE was transferred onto a PVDF membrane by electroblotting (Biometra) for 2 hours at
247 room temperature at 120 V. The membrane was then blocked with blocking buffer [BSA] PBS] for
248 1 hour at room temperature or overnight at 4ºC. Next, the membrane was cleaned three times with
249 washing buffer [PBST]—each time 10 minutes at room temperature, then probed with the
250 conjugated anti-6x His tag® mouse monoclonal antibody (Sigma-Aldrich) overnight at 4ºC or 1
251 hour at room temperature and rewashed three times with washing buffer (CMT; Cat.No
252 CMGWBT). Finally, the protein bands were visualized by staining the membrane with TMB
253 substrate (Promega; Cat.NO W4121).

254 **2.6 Enzyme-Linked Immunosorbent Assay (ELISA)**

255 ELISA plates were coated with total soluble proteins from the wild type and transgenic plants and
256 CCL21 antigen at 37°C for 1 hour, and then incubated with 1% bovine serum albumin (BSA) in
257 PBS for 2 hours at a temperature of 37°C. The wells were washed using PBST/PBS and incubated
258 with the antiserum (conjugated anti-6x His tag® mouse monoclonal antibody), which was
259 reactivated against CCL21 protein (1:1000 dilutions) [35]. Wells were developed with TMB
260 substrate. The color reaction was stopped by H_2SO_4 (2N concentration), and absorbance was read at
261 405 nm wavelength (CMT; Cat.No CMGTMB-100).

262 **2.7 FTIR spectrometry**

263 The sample concentration in KBr should be in the range of approximately 0.2% to 1% [36]. To
264 prepare a KBr tablet, about 8.1 solids and 0.25-0.50 teaspoonful of KBr were thoroughly mixed in a
265 mortar while grinding with the pestle. The material was pressed at 5000-10000 psi by pellet press
266 instrument (following pellet press brochure instructions). The compressed sample was carefully
267 removed from the pellet and placed in the Fourier-transform infrared (FTIR) spectrometer's sample
268 holder. Spectral analysis of UV absorption at 400-4000 cm^{-1} was performed by UNICAM UV 100
269 UV/visible light spectrophotometer. FTIR spectra were recorded on a Thermo Nikolet
270 AVATAR370 spectrometer.

271 **2.8 MALDI TOF/TOF mass spectroscopy**

272 The purified recombinant protein was analyzed for purity by SDS-PAGE stained with G-250
273 Coomassie Blue. Protein spots were excised from preparative stained gels, and Gel slices were
274 destained with wash solution [100% acetonitrile and 50 mM ammonium bicarbonate (NH_4CHO_3)]
275 for 1 hour at room temperature. The protein spot was then air-dried for 30 min at 37°C. Protein was
276 digested using a trypsin solution (12 ng/ml trypsin in 50 mM NH_4CHO_3) by incubation for 45 min
277 at 47°C. Excess of trypsin solution was removed and replaced by 50 mM NH_4CHO_3, and the gel
278 slice was incubated overnight at 37°C [37]. Samples were sent to the Centre of Mass Spectrometry
279 of York University to analyze the plant synthetic protein by conventional ionization methods.

280 **2.9 *In Vitro* wound assay**

In vitro wounds were induced using a modified protocol adapted from Phan *et al*. (2001). Clinical studies have revealed that MCF7 breast cancer tumors do express CCR7 [38]. In order to elucidate the functional role of CCL21/CCR7, MCF7 cells obtained from Razavi Khorasan branch of Academic Center for Education Culture and Research (ACECR) (Mashhad, Iran) were seeded in 6-well plates at densities of 6×150 cells/well in the DMEM high glucose growth medium. After reaching 95% confluency, monolayers of cells were scratched using a sterile pipette tip and the cells drawn firmly across the dish PBS was used for washing the cells to remove the loosened debris/ for washing out non-adherent cells. 7.5 µg/ml of recombinant plant protein, commercial protein (as positive control), and non-recombinant protein (as negative control) were added to each series of wells. Moreover, the cells were treated with an equivalent amount of DMSO as control. For migration assay, cultures were rinsed twice using PBS solution, fixed by absolute methanol, stained by Giemsa, and inspected by a light microscope equipped with a calibrated ocular lens at 40x magnification. Images were recorded 24, 48, and 72 hours after wounding. Cell migration rates were quantified by evaluating the changes in the wound area (pixels) using Image J 1.46 r software.

2.10 MTT cytotoxicity assay

MTT assay was used to determine the half-maximal inhibitory concentration (IC_{50}) of all recombinant protein concentrations in this study. series of dose-response data (e.g. protein concentrations x_1, x_2, ..., x_n and viability percentages y_1, y_2, ..., y_n) were needed for calculating IC50. Y values were ranging from 0 to 1. Therefore, the most precise method for estimating IC_{50} is x-y plotting, followed by fitting the corresponding data with a straight line (linear regression). The IC_{50} value was then estimated using the fitted line [39].

$$Y = a * X + b$$

$$IC50 = (0.5 - b)/a.$$

After being seeded at a density of 8×10^3 cells/well in 96-well plates for 24 hours, the cells were treated with different concentrations of CCL21 recombinant protein, commercial CCL21, and non-recombinant protein (2.5, 5, 7.5, 10 µg/ml for 24, 48, and 72h). Next, 5 mg/ml MTT solution (Sigma, Germany) was added to each well. Plates were incubated at 37°C for 4 hours. Finally, the insoluble formazan was dissolved in DMSO. Optical density of each well was measured spectrophotometrically at 570 nm (all tests were performed in triplicate). The viability of cells in each treatment was calculated by dividing the absorbance of treated cells in each concentration to the mean absorbance of control cells.

2.11 Under agarose gel assay

Under agarose gel assay was used to investigate the mechanism of CCl21 impact on T-cell migration because chemokines are cytokines involved in leukocyte migration [40].

2.11.1 PBMC isolation from whole blood

316 The Ficoll method was used for separating and isolating PBMC[2] (PBMC contain $CD4^+$ and $CD8^+$
317 and CCR7 Expression in Human Primary PBMCs[41]). 10ml Ficoll was added to 4ml blood in a
318 50 ml tube, and then the blood was diluted with 2X phosphate-buffered saline (2X PBS) and 2%
319 fetal bovine serum albumin (2% FBS). Finally, 5 ml of PBS solution was added. Diluted blood rose
320 to the top of Ficoll solution. The tube was centrifuged at room temperature (15-25°C) for 30
321 minutes at 400 g, with the brake in the off position. The upper plasma layers, where the
322 lymphocytes were located, were carefully removed, and the mononuclear/lymphocyte cell layer at
323 the plasma-Ficoll interface was transferred to a clean tube. At least 3x the volume of balanced salt
324 solution was added to the mononuclear/lymphocyte cells in the test tube. The cells were centrifuged
325 at 400 g for 10 minutes at room temperature [42].

326 **2.11.2 Agarose gel well formation for chemotaxis assay**

327 1 percent agarose solution was prepared in a mixture containing 50% DMEM, 10% FBS, 50% PBS,
328 and 2 mM L-glutamine to form wells on the agarose gel. 1.6 mL of the 1% agarose solution was
329 added to each 10-mm sterile petri dish. To humidify the gel, 5 mL DMEM was added to each petri
330 dish after allowing the gel to cool down for 20 min. Afterward, 5 mL FBS-free DMEM was added
331 to the gel (1–6 hours before performing the cell migration assay) and three small wells with a
332 distance of 10 mm were cut in culture medium/ in each petri dish [40, 43].

333 **2.11.3 Chemotaxis Assay and Measurements during Cell Migration**

334 PBMC cells were seeded at a density of 1×10^5 cells in the middle well with 10% FBS-DMEM.
335 After 24 hours, the medium was replaced by FBS-free DMEM [40]. Chemokines (commercial
336 CCL21, recombinant protein) were then placed in one of the neighboring wells to exert their
337 chemoattractant effect, with FBS-free DMEM or non-recombinant protein in other wells as
338 negative controls. Image capture and measurements were performed using an inverted microscope
339 (Olympus).

340 **2.11.4 Cell Processing and Imaging; DAPI staining**

341 For DAPI staining, cell pellets were fixed in 4% paraformaldehyde (PFA) for 8 minutes (Sigma,
342 Germany). Then, each well was washed 3 times (5 minutes for each wash) with 60 µL of 1x PBS
343 for washing the cells. Afterward, the cells were permeabilized with 60µL/well of 0.1% Triton X-
344 100 for 10 minutes and stained with 50µL/well of DAPI (1:2000 dilution, in 1x PBST) (Merck,
345 Germany) for 10 min [40]. The stained cells were then counted using a fluorescent microscope.
346 Chromatin condensation and nuclear fragmentation were the criteria to confirm apoptosis.

347 **3. Results**

348 **3.1 *In silico* analysis**

349 **3.1.1 Recombinant construct properties**

[2] (peripheral blood mononuclear cells)

The final recombinant construct was codon-optimized. Codon Adaptation Index [44] was used for assessing the degree of codon optimization of this construct and for increasing the protein expression level; CAI[3]=1 was selected to support tobacco codon adaptation. A GC content of 48% was accepted as an appropriate expression (Figure 1A). Afterward, the synthetic *ccl21/IL1β* construct was cloned into the binary vector pBI121 [45]. Molecular weight (Mw), isoelectric point (pI) and solubility of the recombinant protein were estimated to be 14,884.5504 Da, 9.377, and 0.8434, respectively. Furthermore, the instability index was 38.03, which showed that it will be stable. The computed half-lives in mammalian, yeast, and *E. coli* cells were more than 30 h, 20 h, and 10 h, respectively. Aliphatic index and GRAVY were predicted to be 49.17 and -1.242, respectively, which showed that this recombinant protein would have hydrophilic properties. The allergenicity of the recombinant protein was assessed, and accuracy of the prediction was 94% at the -0.4 threshold. Therefore, it was deemed not to be allergenic.

3.1.2 Identification and evaluation of suitable epitopes

DNA sequences encoding human CCL21 used in this structure have a DCCL motif, a domain binding to the CCR7 receptor, and a Pan HLA DR-binding epitope (PADRE) peptide sequence covering more than 90% of the HLA alleles. Since their IC50 is less than 50, they can bind to major histocompatibility complex II and I (MHCII/MHCI) molecules. In addition, the VQGEESNDK sequence of human IL-1β is involved in immune responses and has high adjuvant effects. These immunogenic regions of the recombinant protein were thus designed based on T helper lymphocytes [46], cytotoxic T lymphocyte (CTL) epitopes, and MHCI and MHCII. The aforementioned sequence constituted the principal part of the expression cassette. This recombinant protein binds to CCR7 receptors to form a complex which can bind to MHCI and MHCII molecules on T-cells and produce anti-metastatic and cytotoxic effects on cancer cell line chemotactic response in lymphocyte cells. Predicted epitopes of CTLs and THLs were selected based on the percentage of HLA allele coverage (Table 1). Epitopes with HLA coverage above 90% and IC50 below 50 were selected as the best epitopes for binding to MHCI and MHCII molecules. In addition, the BepiPred-2.0 predictions server showed that most of the recombinant protein sequences had a B-cell epitope position with a 0.5 threshold.

3.1.3 Molecular modeling and dynamics simulation of the recombinant protein

A total of ten models were generated using Modeler 9.24, one of which was selected as the most suitable for the rest of the project (Figure 1B). In this project, MD simulations were used for 100 ns to compare the conformational changes of recombinant proteins. Multiple measurements were analyzed throughout the simulation project, chiefly the root mean square deviation (RMSD) and the radius of gyration of the proteins with the time-dependent function of MD/ with MD as the time-dependent function. The results of these calculations for each simulation are shown in Figure 1C. The slope of RMSD increased rapidly in the first 10 ns of MD simulation. After approximately 10000 ps, RMSD reached 1 nm, which means that RMSD is equal to 1.25 nm at 60000 ps. Afterward, RMSD decreased slightly, reached 1.1 nm at 70000 ps, and remained constant until the end of the simulation. These results indicated the stability of the protein structure in this simulation

[3] Codon Adaptation Index

(Figure 1C). Radius of gyration is an indicator of protein structure compactness. It is a concern with how stable secondary structures are compactly packed into the 3D structure of the protein. The lowest radii of gyration and, accordingly, the tightest packing levels/ ratios are characteristic of α/β-proteins. As depicted in Figure 1D, gyration radius of the protein was approximately 2.3 nm at the beginning of the MD simulation, but it decreased rapidly in the next simulation and reached 2.2 at about 10000 ps. The slope of the radius decreased afterward until it reached 2.14 nm at 80000 ps and then remained constant until the end of the simulation, indicating the stability of the protein. In general, the Rg value indicates the compactness of proteins which in turn reflects their stability. The more Rg fluctuates, the less sable is the protein. Hence, it plays a significant role in comparative studies.

3.1.4 Molecular docking and simulation of multi-epitope protein with the CCR7 receptor

As mentioned, the purpose of this project was to investigate the interactions between ligands and CCR7 receptors. As shown in Table 2, molecular docking was performed and the best cluster had a score of -27, with a size of 34 complexes. In addition, Z-score was equal to -2.3. The image of this complex is shown in Figure 1E. The RMSD parameter was used to study the stability of the recombinant protein that bonded to the CCR7 receptor in molecular dynamics simulations and using the RMSD parameter. The corresponding RMSD diagram and the final structure are shown in Figures 1E and 1F. Figure 1E depicts the final structure of the MD complex, and it should be noted that water and membrane molecules have been removed in the image to show the protein structure more clearly. Figure 1F also represents the changes in the RMSD of the docked proteins over the simulation time. As shown in this figure, RMSD increased sharply to 0.4 nm by 10,000 ps and then it decreased and reached 0.3 nm at 15,000 ps, followed by an abrupt increase to 0.6 nm at 20,000 ps. A decrease and increase are observed in the RMSD diagram once again as the simulation continues. At 50,000 ps, the diagram reaches 0.7 nm and remains constant at the same value until the end of simulation, indicating the stabilization of the CCL21/IL1β protein when attached to CCR7 at 50,000 ps during the simulation.

3.1.5 Placement of CCR7-CCL21/IL1β complex inside the membrane

The CCR7 protein is intermembrane and therefore, the CCR7-CCL21/IL1β complex must be simulated inside the plasma membrane. 162 phosphatidylcholine molecules were used for this purpose and formed the membrane structure. Also, a salt concentration of 150 mM NaCl was used to simulate physiological conditions and neutralize the system (the number of sodium and chlorine atoms in these conditions are 47 and 64, respectively). The size of the system created for the length of the system was 8.22268 and 12.94010 nm, respectively. The TIP3P water model was used as a solvent, and the number of water molecules in the system was 17815. Cut-off values for electrostatic and van der Waals interactions were 1.2 and 1 nm, respectively. The pme algorithm was used to calculate long-range electrostatic interactions. The shake algorithm was used to keep the length of the bonds constant (Figure 1G).

3.2 Expression of *ccl21/IL1β* in Transgenic Plants

The regenerated transgenic plants were generation of T0 transgenic plants. Genomic DNA from the leaves of T0 transgenic plants was isolated for PCR analysis. Most of the transgenic tobacco plants had 386 bp PCR products (Figure 2A). The third generation of transgenic plants was studied to select homozygous lines with one copy of this synthetic gene. The phenotype of T0 transgenic

plants was Kanamycin Resistant (Kan R), and the genotype was heterozygous. The plants grown from seeds harvested from self-pollinated T0 transgenic plants were named T1 generation (T1 transgenic plants). The phenotypes of T1 plants were either Kanamycin Resistant (Kan R) or Kanamycin sensitive (Kan r). The ratio of phenotype classes was Kan R: Kan r = 3:1. Of the nine first-generation plants (T0). Four plant in the second generation (T1) had a single copy of the synthetic gene and followed Mendelian segregation rules.

Plants grown from seeds harvested from self-pollinated T1 transgenic plants were named T2 generation (T2 transgenic plants). Of the T2 plants studied in the third generation (T2), the two lines (H2 and E1) did not differentiate in contrast to other lines regarding Kanamycin Resistance. Therefore, these two lines were considered to be third-generation homozygous lines. Moreover, the presence of synthetic construct and *nptII* in T2 plants was evaluated using PCR, and 782 bp bands were observed for DNA samples of transgenic lines (Figure 2B).

3.3 Evaluation of *ccl21/IL1β* expression by real-time PCR assay

The expression of *ccl21* was quantified using quantitative real-time PCR. Three samples from each transgenic line and one from the non-transgenic line (as control) were used for real-time PCR. Results indicated that the foreign gene was transcribed in the transgenic lines (Figure 2C).

3.4 Detection of purified recombinant protein

The expected 55 kDa band was seen on SDS-PAGE for the purified protein sample from the homozygous transgenic line, indicating expression of the recombinant protein in the transgenic lines (Figure 3A).

Dot blot and western blot assays confirmed the expression of recombinant protein. In the dot blot assay, no signal was observed for wild-type plants, whereas expression of the gene of interest in transgenic lines was confirmed (Figure 3B). In western blot analysis, the protein with an estimated molecular weight of 55 kDa was successfully detected (Figure 3C).

Besides, ELISA assay was employed to quantify the expression of recombinant protein, and a standard curve was drawn by ELISA using concentrations of commercial CCL21 (Cat No: 966-6C) over the linear range from 0.25 to 2.5 µg/ml with 0.5 µg/ml increments. The experiment showed that the recombinant protein expression levels were 594 µg/g and 342 µg/g of fresh weight (FW) for two transgenic lines, and these lines were named H2 and E1 respectively. Total Soluble Protein (%TSP) of recombinant protein was measured to be 2.14% and 1.81% for H2 and E1 transgenic lines, respectively. In contrast, no significant differences were observed for non-transgenic plants. Results of ELISA analysis for the expressed recombinant protein from the transgenic lines were in agreement with those of CCL21/IL1β expression analysis conducted by a conjugated anti-His antibody.

3.5 Evolution/ Evaluation of CCL21 secondary structure in commercial, recombinant and non- transgenic protein by FTIR assessment

Secondary structures of commercial CCL21, purified CCL21 recombinant protein, and non-transgenic protein were analyzed by FTIR spectroscopy at 400-4000 cm^{-1}, as illustrated in Figure 4. The recombinant protein showed similar peak positions to the commercial antigen throughout most of the absorption range which indicates that both proteins had a similar molecular structure. However, there was a difference in the OH and NH_2 region (3000-3500 cm^{-1}). Furthermore, a peak at 3430 cm^{-1} in recombinant protein and one at 3425 cm^{-1} in the commercial antigen were observed. Another difference in the two samples was related to the absorption region of the CO amino acid (1500-2000 cm^{-1}). An absorption spectrum of 1645 was observed in the purified recombinant CCL21, while 1639 cm^{1} was observed for the commercial antigen, which could be related to the presence of 9 different amino acids in the recombinant sample which were absent in the commercial antigen. The data revealed many disparities in the different absorption bands of the two plants, indicating that CCL21 has been expressed with 134 amino acids in the transgenic plants and, presumably, that the two samples had different molecular structures. The most important difference is related to the OH and NH_2 region (3000-3500 cm^{-1}). Moreover, a peak at 3423 cm^{-1} in the transgenic line and at 3407 cm^{-1} in non-transgenic tobacco was shown. Another difference was in the CO amino acid absorption region (1500-2000 cm^{-1}). Finally, absorption peaks of 1653 1620 cm^{-1} were observed for the transgenic line and the non-transgenic tobacco plant, respectively, which is due to 134 different amino acids in transgenic samples and could be the main reason for the differences we observed between the transgenic and non-transgenic tobacco plants.

3.6 Analysis of MALDI-TOF/TOF Mass Spectra of the Recombinant Protein

MALDI-TOF/TOF results were analyzed using Mascot software. Searches used the concatenated Mascot Generic Format (mgf) file. Mascot software identified two peptides matching the expected CCL21/IL1β sequences with a high score. Mascot analysis demonstrated that CSIPAILFLPR and VQEESNDK sequences are part of human CCL21 and ILIβ with molecular weights of 1229.55 Da and 947.1 Da, respectively, whereas no tobacco sequences were detected. The average protein sequence coverage was 12%, which confirmed recombinant CCL21/IL1β as the target protein that was correctly expressed and purified from transgenic lines.

3.7 Migration of the cancer cell line into the scratch

The initial width of scratches in cultured cancer cells was estimated between 700 to 800 μm. Cell migration rate in treated groups depended on the applied transgenic tobacco lines. Migration rate of MCF7 cells was estimated in three groups: a group with commercial CCL21 antigen as the positive control, the medium culture group without plant protein extract as the negative control, and the purified protein extract from transgenic tobacco leaves as the third group. Medium concentrations of the extract (7.5 μg/ml) induced migration of the cancer cells and closure of the scratch, and the percentage of closure was calculated using Image J. software. When assessed 24 hours post-treatment, the two control groups had migrated by 22% to scratch. After 48 hours, the scratch closure was 88%. Surprisingly, 72 hours following the same treatment, the scratch was almost completely closed. However, 24 hours after treatment with the same concentration of the purified protein extract of transgenic leaves, no evident migration was detected for the cells; but 15% and 28% scratch closure occurred after 48 and 72 hours, respectively. The results suggest that the

extraction of plant recombinant protein was negatively related to the migration rate of the cells (Figure 5).

3.8 Cytotoxicity of CCL21/IL1β as Recombinant Protein

CCR7+ MCF-7 Human breast cancer cells [13] were treated with different concentrations of CCL21/IL1β recombinant protein, non-recombinant protein as the negative control, CCL21 commercial protein as the positive control, and also DMEM high glucose culture medium as the control, for 24, 48, and 72 hours to investigate the cytotoxicity of CCL21/IL1β using the MTT test. As summarized in Figures 6A to 6C; CCL21/IL1β induced its toxic effects in a dose- and time-dependent manner. 72 hours after treatment with a concentration of 7.5 µg/ml, survival rate of cancer cells incubated with the CCL21/IL1β purified recombinant protein was 28% compared to DMEM (Figure 6A). The IC_{50} of CCL21/IL1β plant recombinant protein against MCF7 cells was 3.86 µg/ml. Interestingly, in comparison with this purified plant recombinant protein different concentrations of commercial CCL21 were used according to the standard curve of %TSP, where CCL21/IL1β antigen promoted its toxic effects at a concentration of 7.5 µg/ml, the survival rate of cancer cells was 22.1%, and IC_{50} was 0.315 µg/ml (Figure 6B). Therefore, various concentrations of commercial CCL21 were used for drawing the standard curve to determine the percentage of TSP of the recombinant protein; and commercial CCL21 antigen at concentrations of 0.2, 0.5, 1, and 2.5 µg/ml were used to determine the maximum amount of antibody. At a concentration of 7.5 µg/ml, survival rate of cancer cells incubated with non-recombinant protein was 74.3% lower compared to DMEM as control (Figure 6C).

3.9 Migration of PBMC cells (Chemotaxis Assay)

CCR7 cytokine is expressed in human primary PBMCs, to observe whether PBMC cells and chemoattractants attract each other, PBMC cells can be seeded in the middle well and chemoreactants in the wells to its right and left [43]. Four versions of simultaneous migration induction groups were used in this experiment. The first group was the simultaneous stimulation of commercial CCL21 as the positive control (2.5 µg/mL) in the left well and DMEM medium as the negative control (2.5 µg/mL) in the right one. The results confirmed that T-cells responded similarly to CCL21/IL1β stimulations. As a result, we obtained approximately 170 migrating cells after 24 hours of stimulation (Figure 7 A). Migration kinetics were also very similar for CCL21/IL1β recombinant protein and the non-recombinant protein. Therefore, we estimated that approximately 138 cells migrated within 24 hours (Figure 7 B).

For the other group, FBS 10% was placed (2.5 µg/mL) in the left well as the positive control, and DMEM medium as the negative control (2.5 µg/mL) in the right one, as depicted in Figure 7 C. The result was the migration of 158 cells after 24 hours to the left well. The last group had two negative controls: one well was filled with non-recombinant protein, and the other with DMEM medium. Only a few cells (15 cells) were observed in each well, implying that neither chemoattractant factor had absorbed the cells (Figure 7 D). An approximate quantification of the number of migrated cells was achieved using the Heit and Kubes method [47]. In this analysis, the number of migrated cells in the distance of wells containing cells and those containing chemoattractants was deduced from the number of cells that migrated between the wells containing cells and the wells containing non-

552 absorbent material.Consequently, as shown in Figure 7, the number of monocytes moving toward
553 the adsorbent substance was higher than that toward the non-adsorbent material, and the chemotaxis
554 of the recombinant protein was estimated to be about 91% (Table 3). This modified methodology
555 allowed us to stain the nuclei of live cells by DAPI staining and use fluorescence microscopy to
556 overcome the issue of low contrast between the agar background and the cells. However, in our
557 experience, about 50% to 70% of the migrating cells might be lost due to cell staining (Figures 7E
558 to 7I). Therefore, by examining the PBMC cells that had migrated toward the commercial CCL21,
559 the recombinant plant CCL21, and 10% FBS (as the growth factor), we found that CCL21 is a
560 chemokine with chemokinetic properties leading to the migration of immune cells.With this initial
561 test, thus, it was possible to determine the role of CCL21/IL1β in migration and movement of
562 immune cells towards tumor cells. Furthermore, comparison of chemotaxis (CT) and chemokinesis
563 (CK) confirmed that there is no difference in cell migration toward CCL21 recombinant protein as
564 chemokinesis and growth factor as chemotaxis was considered (Figures 7J and 7K).

565

566 **4. Discussion**

567 This research aimed at designing a codon-optimized *ccl21/IL1β* gene from human gene *ccl21* and
568 the *interleukin-1 beta* adjuvant sequence VQGEESNDK, as well as examining the stability and
569 binding affinity of this recombinant construct and CCR7 receptors through *in silico* analyses. The
570 synthesized construct was introduced into tobacco plants, and expression, structure, and function of
571 this recombinant protein were assessed. Since these two are human genes, and human is a very
572 different organism from tobacco, the sequence was optimized for maximal protein expression in the
573 selected host. Molecular dynamics simulation and various analyses were used to identify these two
574 optimized genes [28]. Furthermore, ClusPro software was used to investigate the interaction
575 between cytokine ligands and CCR7 receptors. The best cluster had a Z-Score of -2.3. The stability
576 and flexibility of this recombinant protein were determined by MD simulation, and RMSD
577 remained constant until the end of the simulation.

578 In SDS PAGE, dot blotting and western blotting assays, the purified protein sample from transgenic
579 leaves generated a strong signal comparable to the positive control, whereas the protein from wild
580 type plant was not detectable.

581 In previous studies on expression of other recombinant proteins in tobacco plants, TSP yields of
582 0.019–0.31% were reported [48, 49]. In this work, however, CCL21/IL1β was expressed in the
583 transgenic tobacco lines at levels up to 1.81–2.14% of TSP, and also ELISA results demonstrated
584 that CCL21/IL1β has been correctly expressed and folded in tobacco plants and was fully
585 functional.

586 FTIR was used to investigate the structure of the recombinant protein and to ensure the insertion
587 and expression of the foreign gene into the tobacco plants. FTIR assessment confirmed the presence
588 of the recombinant protein (and thus the synthetic construct) in transgenic leaves of tobacco.
589 Commercial CCL21 had a similar peak profile in most of the absorption areas of the spectra. Put
590 together, these two sets of data indicate that both proteins had a similar molecular structure even
591 though there was a high dissimilarity in peak positions between transgenic and non-transgenic

592 tobacco. FTIR measurement and MALDI-TOF/TOF mass spectrum assessments confirmed that
593 *ccl21/IL1β* was correctly expressed in the tobacco plant.

594 We also investigated the potential of the purified recombinant protein for stimulating the
595 proliferation and migration of cancer cells by the wound healing method [45, 50, 51]. Cancer cell
596 lines migrated into the wound site 24 hours after seeding cells in the MCF7 growth medium (15%
597 FBS). However, after replacing the growth media with a medium with different CCL21/IL1β
598 protein treatments, the purified protein extract from transgenic leaves and the commercial protein
599 remarkably prevented the migration and growth of cancer cell lines in monolayer cell cultures
600 compared to control groups (basal medium and non-recombinant protein). Furthermore, the results
601 demonstrated a decrease in the survival rate and metastasization of cancer cells in the presence of
602 CCL21 recombinant protein.

603 The MTT assay was utilized to evaluate the cytotoxicity of CCL21/IL1β on cancer cells. In this
604 method, the yellow tetrazolium MTT (3-(4, 5-dimethyl thiazolyl-2)-2, 5-diphenyltetrazolium
605 bromide) is reduced by metabolically active cells. The MTT assay measures the cell proliferation
606 rate, and cytotoxicity leads to reduced cell viability and apoptosis [52]. MTT results showed that
607 the IC_{50} of CCL21/IL1β on MCF7 cells was less than that of the non-recombinant protein. In
608 addition, toxicity of commercial CCL21 on MCF7 cells was similar to CCL21/IL1β recombinant
609 protein, which is the anticancer antigen used for lung cancer treatment [53]. Monitoring
610 CCL21/IL1β activity for 72 hours showed that the two components act in a dose and time-
611 dependent manner. Chemotactic abilities could be measured using different criteria, such as the
612 number of attracted cells, induced speed, and morphological features [54]. The chemokinetic
613 activity of this recombinant protein in stimulating cell motility and chemotactic movement of
614 PBMC cell populations was investigated by agarose assay. Agarose assay has been used for
615 studying cellular chemotactic reactions and the signaling processes underlying them [54],[55].
616 Generally speaking, chemokinesis is a chemically induced motile response of unicellular organisms
617 to chemical materials that proved the cells to alter their migratory behaviors. However,
618 chemokinesis has a a more random nature compared to chemotaxis [47]. Hence, the results of our
619 study demonstrate a differentiation between chemokinetic (CCL21) and chemotactic (FBS)
620 movement. It is expected that this recombinant multi-epitope protein can be considered for cancer
621 treatment. It can also treat viral diseases, such as AIDS and coronaviruses (e.g. Covid-19) since it
622 triggers the immune system to produce potent antibodies in patients with these diseases.

623 **5. Conclusion**

624 Chemotherapy is a method mainly used for treating cancer, which unfortunately causes adverse side
625 effects such as hair loss, nausea, and weakness. complications occur because cancer treatment aims
626 to kill cancer cells, and some of the body's healthy cells are also damaged in the process. For
627 example, one of the drugs prescribed to most cancer patients is Herceptin which, in addition to its
628 high cost, weakens the immune system and causes many side effects. Recombinant proteins,
629 however, can be produced at a minimal cost and have no particular side effects, strengthening the
630 immune system and immunizing the patient before chemotherapy. In addition, many of the drugs
631 that have been suggested for treatment of viral diseases, such as AIDS and coronaviral conditions,
632 produce potent antibodies in the body, which can stimulate the immune system of the patient. So

far, many commercial drugs have been designed and produced for stimulating and strengthening the patient's immune system. Commercial drugs based on CCL21 are also available in the market. The International Cancer Institute now recognizes CCL21 as an effective drug in the treatment of AIDS and cancer. However, these drugs have limitations in immunotherapy. For example, CCL21 only affects T-lymphocytes and CTLs and reduces regulatory T-cells (Tregs) expression and has no role in B-lymphocytes, macrophages, and neutrophils. The recombinant drug produced in this study does not have any special chemical side effects and will certainly not cost much if it is commercialized. If successful in the clinical phase. To the best of our knowledge, this study is the first to report expression of *ccl21/IL1β* construct in tobacco via agrobacterium gene transformation method and high-level expression of CCL21/IL1β. The cost of producing this recombinant drug is very low compared to the commercial antigen. The experiments confirmed that the recombinant protein has epitope sequences covering more than 90% of the HLA-DRB4 allele. Therefore, this recombinant protein is presented by APCs after binding and endocytosed through the CCR7 receptor. This antigen-receptor complex induces efficient CD4+ T-cell responses by the MHC class I and II antigen processing pathways. Furthermore, it is a potential option in the immunotherapy of cancer.

Acknowledgments This study was financially supported by the Biotechnology Development Council of the Islamic Republic of Iran. We would also like to thank Stem Cells and Regenerative Medicine Research Group, the Academic Center for Education, Culture, and Research (ACECR), Razavi Khorasan Branch, Mashhad, Iran.

Authors' contributions MB and HM contributed to designing the research, conducting the experiments, and data analysis.

Funding The research was financed by the Office of Vice President for Research and Technology of Ferdowsi University of Mashhad, Iran, Stem Cells and Regenerative Medicine Research Group, the Academic Center for Education, Culture, and Research.

Availability of data and material All data, materials, and methods are presented in the manuscript.

Conflict of interest The authors declare that they have no conflict of interest.

Ethics approval This project was ethically approved in accordance with Code IR.MUMS.REC.1399.428.

Consent to participate Not applicable.

Consent for publication Not applicable.

Code availability Not applicable.

References

Uncategorized References

668 .1 Akhter, N., et al., *Probiotics and prebiotics associated with aquaculture: a review.* Fish & shellfish
669 immunology, 2015. **45**(2): p. 733-741.
670 .2 Moore, M.A., *The role of chemoattraction in cancer metastases.* Bioessays, 2001. **23**(8): p. 674-676.
671 .3 Jorgensen, A.S., et al., *Biased signaling of CCL21 and CCL19 does not rely on N-terminal*
672 *differences, but markedly on the chemokine core domains and extracellular loop 2 of CCR7.*
673 Frontiers in immunology, 2019. **10**: p. 2156.
674 .4 Chen, Y., et al., *CCL21/CCR7 interaction promotes EMT and enhances the stemness of OSCC via a*
675 *JAK2/STAT3 signaling pathway.* Journal of Cellular Physiology, 2020.
676 .5 De Biasi, S., et al., *Marked T cell activation, senescence, exhaustion and skewing towards TH17 in*
677 *patients with COVID-19 pneumonia.* Nature communications, 2020. **11**(1): p. 1-17.
678 .6 Van Raemdonck, K., et al., *CCL21/CCR7 signaling in macrophages promotes joint inflammation*
679 *and Th17-mediated osteoclast formation in rheumatoid arthritis.* Cellular and Molecular Life
680 Sciences, 2020. **77** :(7)p. 1387-1399.
681 .7 Zhao, D.-x., et al., *Enhanced antitumor immunity is elicited by adenovirus-mediated gene transfer of*
682 *CCL21 and IL-15 in murine colon carcinomas.* Cellular immunology, 2014. **289**(1): p. 155-161.
683 .8 Joutoku, Z., et al., *CCL21/CCR7 axis regulating juvenile cartilage repair can enhance cartilage*
684 *healing in adults.* Scientific reports, 2019. **9**(1): p. 5165.
685 .9 Cyster, J.G., *Chemokines and the homing of dendritic cells to the T cell areas of lymphoid organs.*
686 Journal of Experimental Medicine, 1 :(3)189 .999p. 447-450.
687 .10 Gollmer, K., et al., *CCL21 mediates CD4+ T-cell costimulation via a DOCK2/Rac-dependent*
688 *pathway.* Blood, 2009. **114**(3): p. 580-588.
689 .11 Beemiller, P., J. Jacobelli, and M.F. Krummel, *Integration of the movement of signaling*
690 *microclusters with cellular motility in immunological synapses.* Nature immunology, 2012. **13**(8): p.
691 787-795.
692 .12 Westmeier, J., et al., *Impaired cytotoxic CD8+ T cell response in elderly COVID-19 patients.* mBio,
693 2020. **11**(5.(
694 .13 Wu, S., et al., *CC chemokine ligand 21 enhances the immunogenicity of the breast cancer cell line*
695 *MCF-7 upon assistance of TLR2.* Carcinogenesis, 2011. **32**(3): p. 296-304.
696 .14 Floss, D.M., et al., *Biochemical and functional characterization of anti-HIV antibody–ELP fusion*
697 *proteins from transgenic plants.* Plant Biotechnology Journal, 2008. **6**(4): p. 379-391.
698 .15 Van Damme, J., et al., *Homogeneous interferon-inducing 22K factor is related to endogenous*
699 *pyrogen and interleukin-1.* Nature, 1985. **314**(6008): p. 266-268.
700 .16 Boraschi, D., A. Tagliabue, and A.D. Miller, *The immunostimulatory effect of IL-1β in vivo is*
701 *blocked by antisense peptides complementary to the loop sequence 163–171.* FEBS letters, 2009.
702 **583**(4): p. 792-796.
703 .17 Morris, D.L., et al., *Unraveling multiple MHC gene associations with systemic lupus erythematosus:*
704 *model choice indicates a role for HLA alleles and non-HLA genes in Europeans.* The American
705 Journal of Human Genetics, 2012. **91**(5): p. 778-793.
706 .18 Schiavo, R., et al., *Chemokine receptor targeting efficiently directs antigens to MHC class I*
707 *pathways and elicits antigen-specific CD8+ T-cell responses.* Blood, 2006. **107**(12): p. 4597-4605.
708 .19 Occhialini, A., et al., *Mini-synplastomes for plastid genetic engineering.* Plant Biotechnology
709 Journal, 2021.
710 .20 Fischer, R., et al ,.*Plant-based production of biopharmaceuticals.* Current opinion in plant biology,
711 2004. **7**(2): p. 152-158.
712 .21 Beihaghi, M., et al., *Transient Expression of CCL21Chemokine in Tobacco via Agroinfiltration.*
713 International Journal of Scientific and Engineering Research, 2016. **7**.
714 .22 Srinivasan, A., et al., *Preclinical development of plant-based oral immune modulatory therapy for*
715 *haemophilia B.* Plant Biotechnology Journal, 2021.
716 .23 Day, A. and M. Goldschmidt-Clermont, *The chloroplast transformation toolbox: selectable markers*
717 *and marker removal.* Plant biotechnology journal, 2011. **9**(5): p. 540-553.
718 .24 Kudla, G., et al., *Coding-sequence determinants of gene expression in Escherichia coli.* science,
719 2009. **324**(5924): p. 255-258.
720 .25 Nguyen-Hoai, T., et al., *CCL21*) *SLC) improves tumor protection by a DNA vaccine in a Her2/neu*
721 *mouse tumor model.* Cancer gene therapy, 2012. **19**(1): p. 69-76.

.26 Musiani, F., et al., *Molecular dynamics simulations identify time scale of conformational changes responsible for conformational selection in molecular recognition of HIV-1 transactivation responsive RNA.* Journal of the American Chemical Society, 2014. **136**(44): p. 15631-15637.

.27 Acevedo, G.R., et al., *In Silico Guided Discovery of Novel Class I and II Trypanosoma cruzi Epitopes Recognized by T Cells from Chagas' Disease Patients.* The Journal of Immunology, 2020. **204**(6): p. 1571-1581.

.28 Gaieb, Z. and D. Morikis, *Detection of Side Chain Rearrangements Mediating the Motions of Transmembrane Helices in Molecular Dynamics Simulations of G Protein-Coupled Receptors.* Computational and structural biotechnology journal, 2017. **15**: p. 131-137.

.29 Safavi, A., et al., *In silico analysis of transmembrane protein 31 (TMEM31) antigen to design novel multiepitope peptide and DNA cancer vaccines against melanoma.* Molecular immunology, 2019. **112**: p. 93-102.

.30 O'Donnell, T.J., A. Rubinsteyn, and U. Laserson, *MHCflurry 2.0: Improved Pan-Allele Prediction of MHC Class I-Presented Peptides by Incorporating Antigen Processing.* Cell Systems, 202 .0 :(1)11p. 42-48. e7.

.31 Dellafiora, L., et al., *An in silico structural approach to characterize human and rainbow trout estrogenicity of mycotoxins: Proof of concept study using zearalenone and alternariol.* Food chemistry, 2020. **312**: p. 126088.

.32 Topping, J.F., *Tobacco transformation.* Plant Virology Protocols: From Virus Isolation to Transgenic Resistance, 1998: p. 365-372.

.33 Zhang, X., et al., *Establishment of an Agrobacterium-mediated genetic transformation and CRISPR/Cas9-mediated targeted mutagenesis in Hemp (Cannabis Sativa L.).* Plant biotechnology journal, 2021.

.34 Gallois, P. and P. Marinho, *Leaf disk transformation using Agrobacterium tumefaciens-expression of heterologous genes in tobacco*, in *Plant gene transfer and expression protocols* ,1995 .Springer. p. 39-48.

.35 Su, M., et al., *A recombinant nucleocapsid protein-based indirect enzyme-linked immunosorbent assay to detect antibodies against porcine deltacoronavirus.* Journal of Veterinary Medical Science, 2015: p. 15-0533.

.36 Gordon ,S.H., R.E. Harry-O'kuru, and A.A. Mohamed, *Elimination of interference from water in KBr disk FT-IR spectra of solid biomaterials by chemometrics solved with kinetic modeling.* Talanta, 2017. **174**: p. 587-598.

.37 Ghabooli, M., et al., *Proteomics study reveals the molecular mechanisms underlying water stress tolerance.* 2013.

.38 Rizeq, B. and M.I. Malki, *The Role of CCL21/CCR7 Chemokine Axis in Breast Cancer Progression.* Cancers, 2020. **12**(4): p. 1036.

.39 Sebaugh, J., *Guidelines for accurate EC50/IC50 estimation.* Pharmaceutical statistics, 2011. **10**(2): p. 128-134.

.40 Heit, B. and P. Kubes, *Measuring chemotaxis and chemokinesis: the under-agarose cell migration assay.* Science's STKE, 2003. **2003**(170): p. pl5-pl5.

.41 Mullen, K.M., et al., *Expression of CCR7 and CD45RA in CD4+ and CD8+ subsets in cerebrospinal fluid of 134 patients with inflammatory and non-inflammatory neurological diseases.* Journal of neuroimmunology, 2012. **249**(1-2): p. 86-92.

.42 Higdon, L.E., et al., *Virtual global transplant laboratory standard operating procedures for blood collection, PBMC isolation, and storage.* Transplantation direct, 2016. **2**(9.(

.43 Mousseau, Y., et al., *Improved agarose gel assay for quantification of growth factor-induced cell motility.* Biotechniques, 2007. **43**(4 :(p. 509-516.

.44 Zou, Y., et al., *CCL21 as an independent favorable prognostic factor for stage III/IV colorectal cancer.* Oncology reports, 2013. **30**(2): p. 659-666.

.45 Beihaghi, M., et al., *Transient expression of CCL21as recombinant protein in tomato .* Biotechnology reports, 2018. **17**: p. 10-15.

.46 Hefferon, K., *Clinical trials fuel the promise of plant-derived vaccines.* Am J Clin Med, 2010. **7**: p. 30-7.

.47 Heit, B. and P. Kubes, *Measuring chemotaxis and chemokinesis: the under-agarose cell migration assay.* Sci. STKE, 2003. **2003**(170): p. pl5-pl5.

.48 Joensuu, J., V. Niklander-Teeri, and J. Brandle, *Transgenic plants for animal health: plant-made vaccine antigens for animal infectious disease control.* Phytochemistry Reviews, 2008. **7**(3): p. 553-577.

.49 Ghiasi, S.M., et al., *Molecular farming, an effective system for the production of immunogenic Crimean-Congo Hemorrhagic fever virus glycoprotein.* Progress in Biological Sciences, 2012. **2**(1): p. 12-29.

.50 Cheng, S., et al., *Crk-like adapter protein regulates CCL19/CCR7-mediated epithelial-to-mesenchymal transition via ERK signaling pathway in epithelial ovarian carcinomas.* Medical oncology, 2015. **32**(3): p. 1-7.

.51 Zubair, M., et al., *Promotion of wound healing by Plantago major L. leaf extracts–ex-vivo experiments confirm experiences from traditional medicine.* Natural product research, 2016. **30**(5): p. 622-624.

.52 Riss, T.L., et al., *Cell viability assays.* 2016.

.53 Mo, M., et al., *CCL21/CCR7 enhances the proliferation, migration, and invasion of human bladder cancer T24 cells.* PloS one, 2015. **10**(3): p. e0119506.

.54 Pietrosimone, K.M., et al., *Measurement of cellular chemotaxis with ECIS/Taxis.* Journal of visualized experiments: JoVE, 2012(62.(

.55 Pietrosimone, K.M., et al., *In Vitro Assays of Chemotaxis as a Window into Mechanisms of Toxicant-Induced Immunomodulation.* Current protocols in toxicology, 2013: p. 18.17. 1-18.17. 24.

MHCI			MHCII		
Epitope peptide	HLA allel	score	Epitope peptide	HLA allel	IC50
IPAKVVRSY	HLA-B*35:01	99.4%	LWVQQLMQH	HLA-DRB4*01:01	15.60
LPRKRSQAEL	HLA-B*07:02	95.7%	ELWVQQLMQ	HLA-DRB4*01:01	17.10
LCADPKELW	HLA-B*58:01	95.4%	PKELW VQQ	HLA-DRB4*01:01	18.50
LCADPKELW	HLA-B*57:01	93.4%	AKVVRSYRK	HLA-DRB4*01:01	19.20
IPAKVVRSY	HLA-B*53:01	90.3%	QQLMQHLDK	HLA-DRB4*01:01	21.40

Table 1. Prediction of T-cell epitopes of CCL21/IL1β protein. A covering score over 90% and IC50 below 50 were used for selecting the best binder epitopes of MHCI and MHCII-related HLAs.

Table2. The best cluster of molecular docking results

Cluster	DOCK score	Cluster size	Z-Score
1	-27	34	-2.3

Table 3. The approximate count of migrated cells and the percentage of chemotaxis according to Figures 7A to 7D [40].

Adsorbent substance	Number of cells in the well containing cells and absorbent material	Number of cells in the well containing cells and non-absorbent material	Chemotaxis rate/ Number of migrated cells	Chemotaxis percentage
Commercial CCL21 (positive control as chemokine)	170	17	153	90
Recombinant CCL21/IL1β	138	12	126	**91**
FBS10% (positive control as chemotactic agent)	158	17	141	89

Chemotaxis rate = (Number of cells in the well containing cells and absorbent material) – (Number of cells in the well containing cells and non-absorbent material)

Percentage of chomotoxicity = (Number of cells in the well containing cells and absorbent material/chemotaxis rate) × 100[43]

A

B

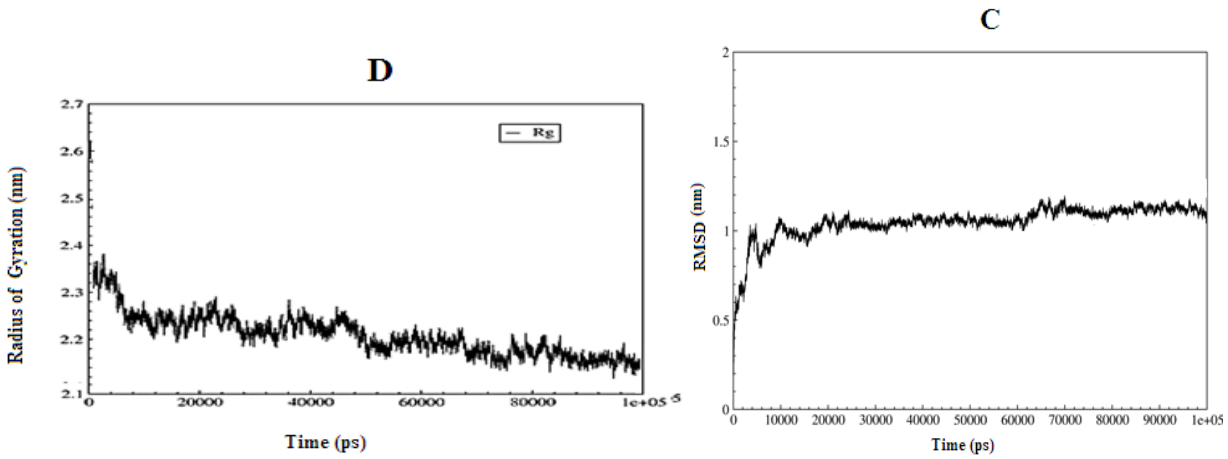

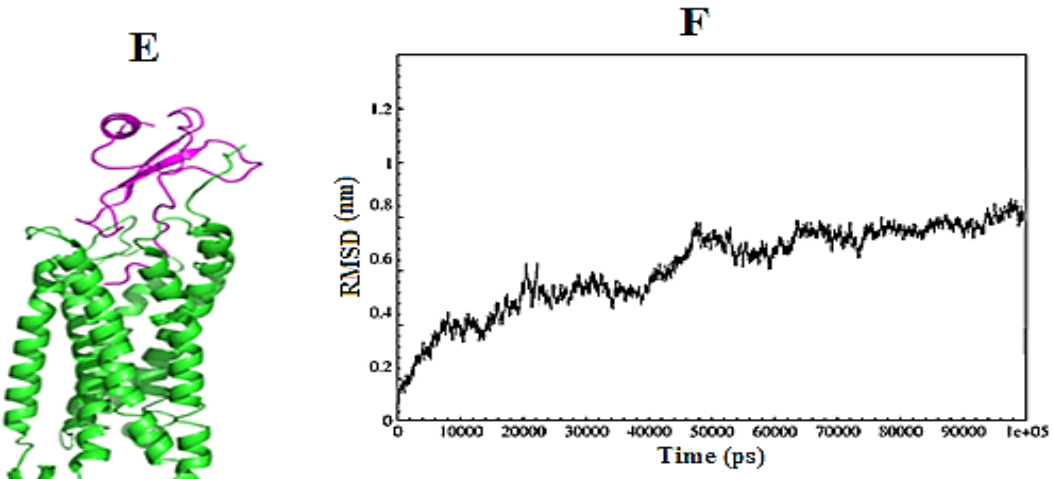

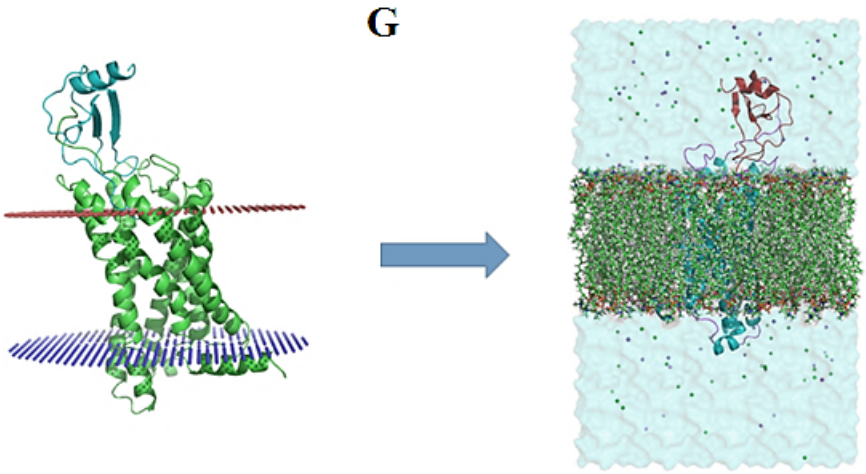

Figure 1. *In silico* analysis of the recombinant protein. **A:** Schematic representation of the pBI121-*ccl21/IL1β* construct. **B:** The best model for the recombinant protein as designed by Modeler 9.24. **C:** RMSD values in MD simulation of the recombinant protein: RMSD slope increased rapidly in the first 10 ns of MD simulation. RMSD reached 1 nm after about 10 ns, and 1.25 nm at 60 ns. Afterward, RMSD decreased slightly, reached 1.1 nm at 70 ns, and remained constant until the end of simulation. **D:** RG values in MD simulation of the recombinant protein: protein's

RG was about 2.3 nm, but it decreases rapidly in the following simulation, reaching 2.2 at about 10 ns, after which the slope of the radius decreased, and RG reached approximately 2.14 nm at about 80 ns. RG then remained constant until the end of the simulation, indicating the stability of the protein. **E:** Molecular docking image of the recombinant protein and CCR7 receptor. **F:** RMSD values in MD simulation of CCR7 and recombinant protein complex; RMSD increased at the beginning of the simulation. After 100 ns, RMSD reached 0.7 nm, after which it remained constant until the end of simulation. **G:** Placement of CCR7-CCL21/IL1β complex inside the membrane by CHARMM-GUI server. This complex must first be located inside the plasma membrane. the number of phospholipids used in the membrane structure was 162 molecules of phosphatidylcholine.

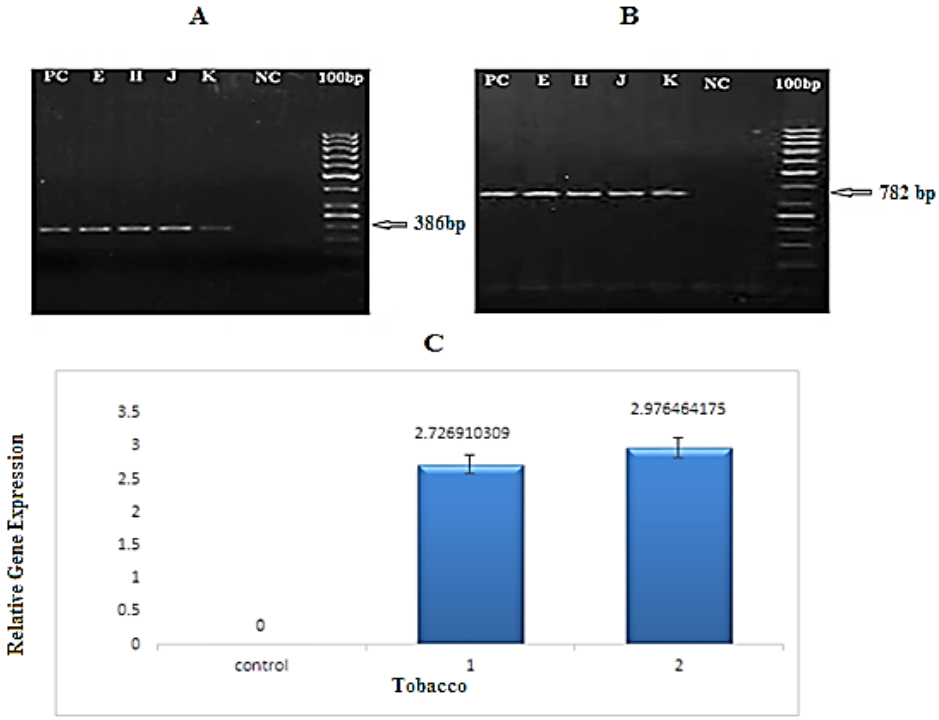

Figure 2. PCR and real-time PCR analysis of *21/Il1β* gene in transgenic tobacco plants**. A:** PCR product of *ccl21/Il1β* in T0 transgenic lines amplified by *CaMV-ccl21* primers (386bp). **B:** PCR product of *ccl21/Il1β* in T2 transgenic lines amplified by *nptII* primers (798 bp). (M: 100bp size marker. NC: PCR product of wild-type plant as negative control. H, J, K, and E: PCR products of transgenic plants. PC: PCR product of pBI121-*ccl21* construct as positive control). **C:** Quantitative measurement of *ccl21/Il1β1* transcription in transgenic lines of tobacco via real time-PCR. 1 and 2: two samples from transgenic lines; Control: negative control (non-transgenic plant).

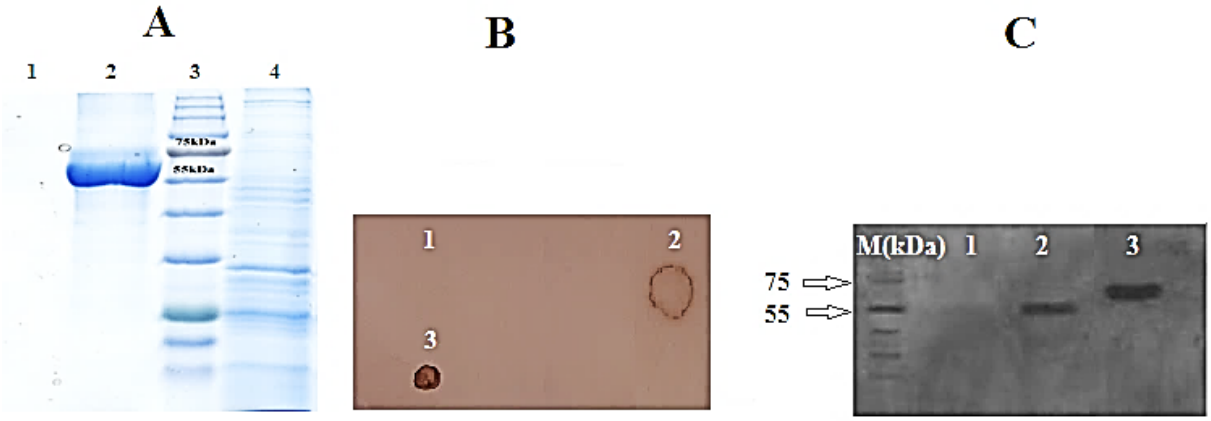

Figure 3. Detection of purified recombinant protein. **A:** SDS-PAGE of purified protein from transgenic lines and non-transgenic tobacco. Lane 1: non-transgenic tobacco as negative control; Lane 2: transgenic line; Lane 3: Fermentase Prestained Protein Ladder (SM1811); Lane 4: total soluble protein. **B:** Dot blot of recombinant protein from transgenic tobacco leaves. **C:** Western blot of CCL21 protein from transgenic tobacco leaves using conjugated anti-6x His tag® mouse monoclonal antibody (Sigma-Aldrich). A clear 55 kDa band was observed for homozygous lines and a 65 kDa band for commercial CCl21 antigens. M: Fermentase Prestained Protein Ladder (SM1811), 1: protein from non-transgenic plant as negative control; 2: protein sample from transgenic plant; 3: Commercial CCL21 antigen (Cat No: 966-6C) as positive control.

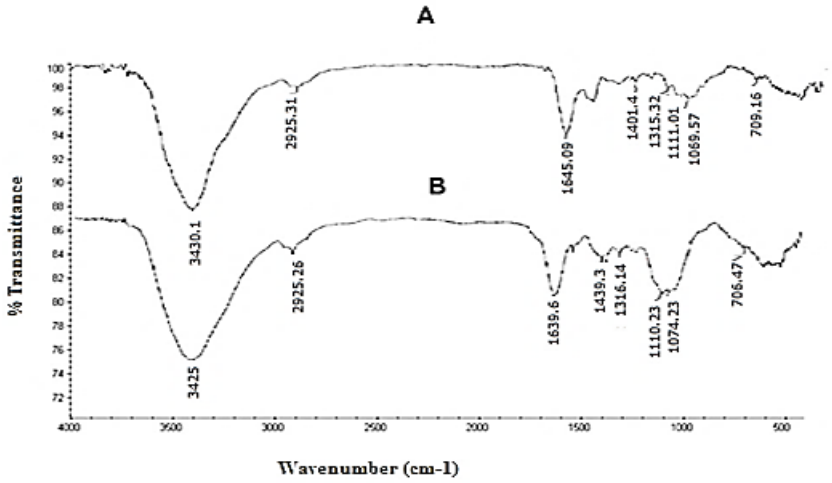

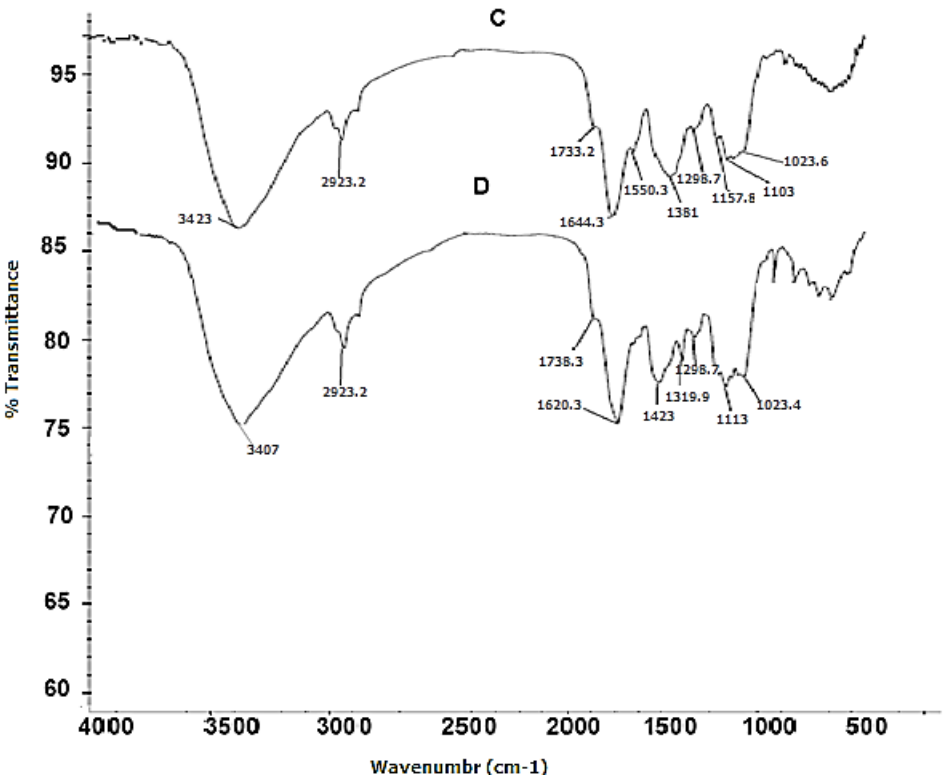

Figure 4. Structure analysis of purified recombinant protein (A) and CCL21 antigen (B), transgenic line (C) and non-transgenic line (D) by FTIR. Similar peak positions were observed in the spectra of A and B; differences can be observed in 3000-3500 cm^{-1} region(the peak at 3430 cm^{-1} in A and the peak at 3425 cm^{-1} in B), which are related to OH and NH_2 in B. CO carbonyl (1500-2000 cm^{-1}) has an absorption spectrum of 1645 in purified A, while corresponding value is 1639 cm^{-1} in B. The spectra showed different peak positions in C and D; the peak was at 3423 cm^{-1} in D and 3407cm^{-1} in C. The absorption spectrum was 1653 in D and 1620 cm^{-1} in C.

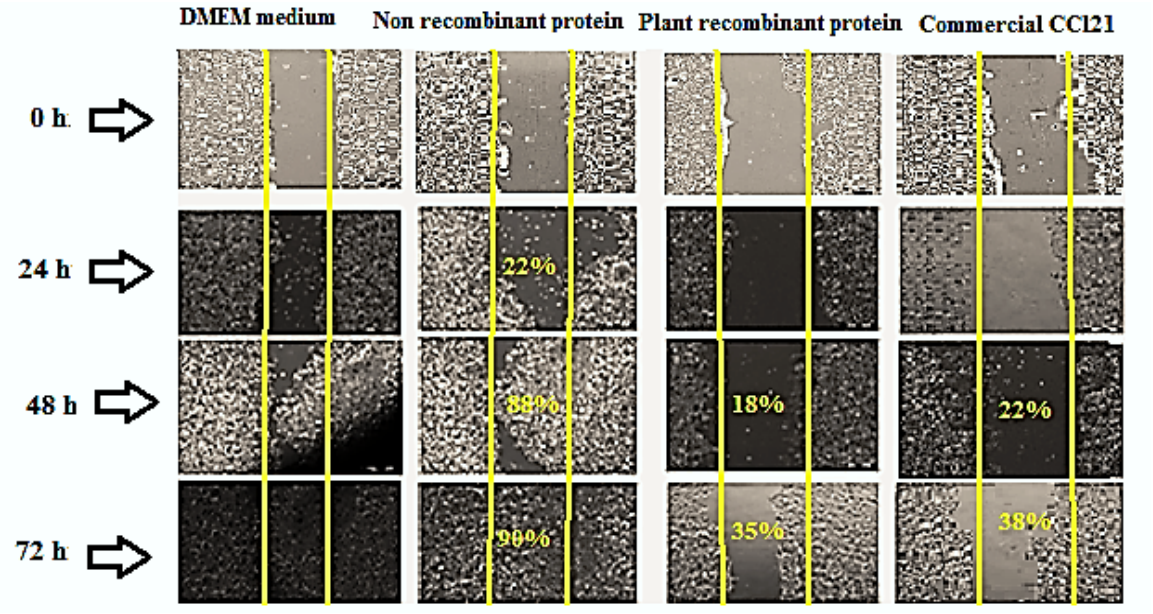

Figure 5. Photomicrographs of *in vitro* wound assay. The initial width of scratches in cancer cell cultures was estimated between 700 to 800 µm. MCF7 migration rates were assessed at 0, 24, 48, and 72 hours after wound induction in each group. Treatments were non-recombinant protein extract and DMEM culture medium as negative controls, plant recombinant protein, and commercial CCl21 as the positive control. Medium concentrations of the extract (7.5 µg/ml) induced migration of cancer cells and closure of the scratch, and closure percentage was calculated using Image J. software. When assessed 24 hours post-treatment, the two control groups had 22% migration to the scratch area. After 48 hours, 88% scratch closure was observed. Surprisingly, 72 hours following the same treatment, the scratch was almost completely closed. With the same concentration of the purified protein extract of transgenic leaves, however, no noticeable migration of the cells was detected 24 hours after treatment, and 15% and 28% scratch closure rates occurred after 48 and 72 hours, respectively.

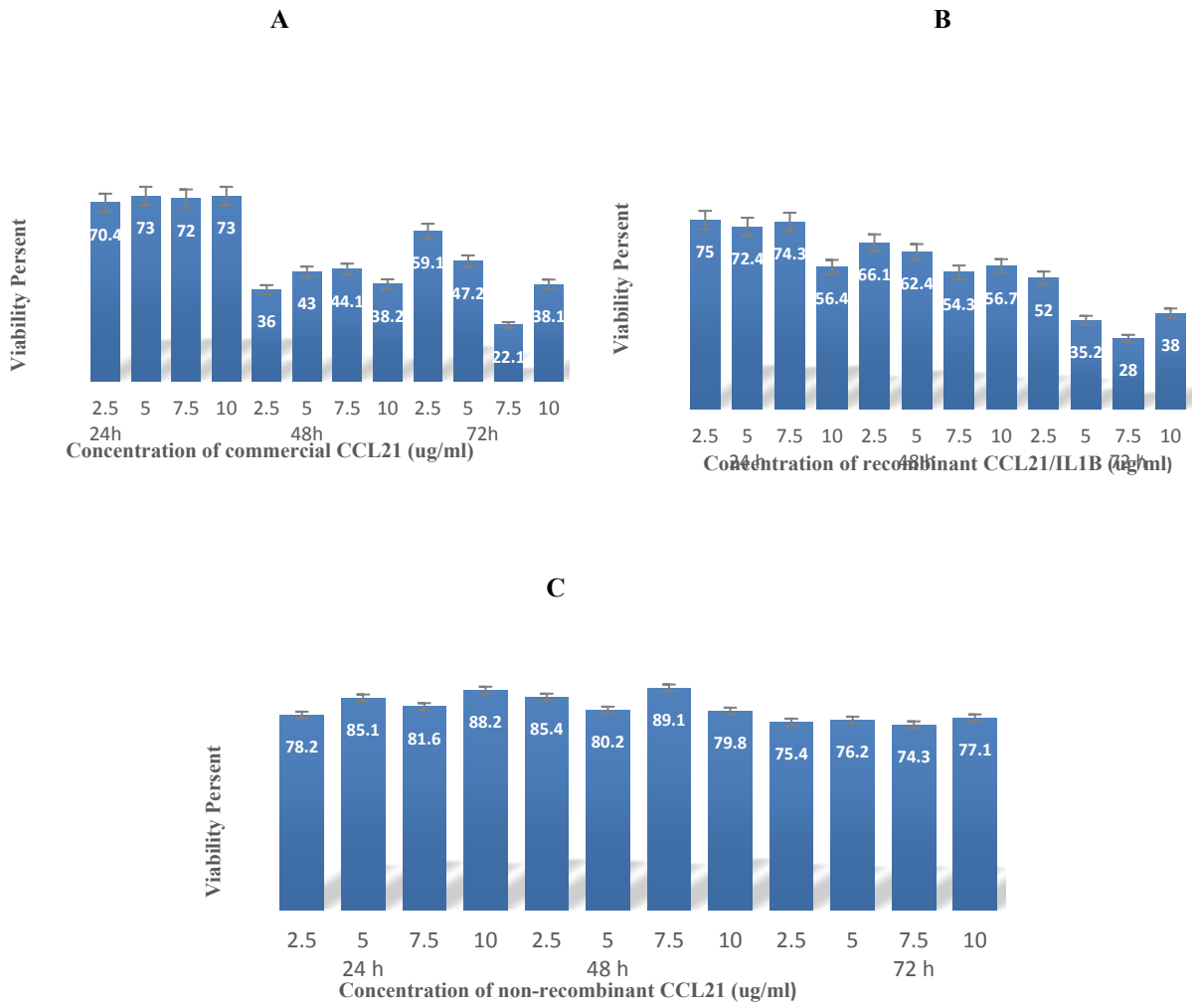

Figure 6. Cytotoxicity analysis of recombinant, commercial, and non-recombinant CCL21 on MCF7 cell line at 24, 48, and 72 hours after incubation. **A:** Cytotoxicity of recombinant CCL21 protein in comparison with the control group at different concentrations (2.5, 5, 7.5, and 10 µg/ml) on MCF7 cancer cells: at 7.5 µg/ml, the survival rate of cancer cells incubated with the purified recombinant CCL21 protein was 22.1% lower in comparison with DMEM medium as the control treatment (MTT assay was performed during 3 consecutive days with 3 different concentrations of recombinant CCL21). **B:** Cytotoxicity of commercial CCL21 protein at different concentrations (2.5, 5, 7.5, and 10 µg/ml) on MCF7 cancer cells was 28% lower in comparison with the control treatment. **C:** Survival rate of cancer cells incubated with 7.5µg/ml commercial CCL21 was 78% lower in comparison with DMEM medium as the control treatment.

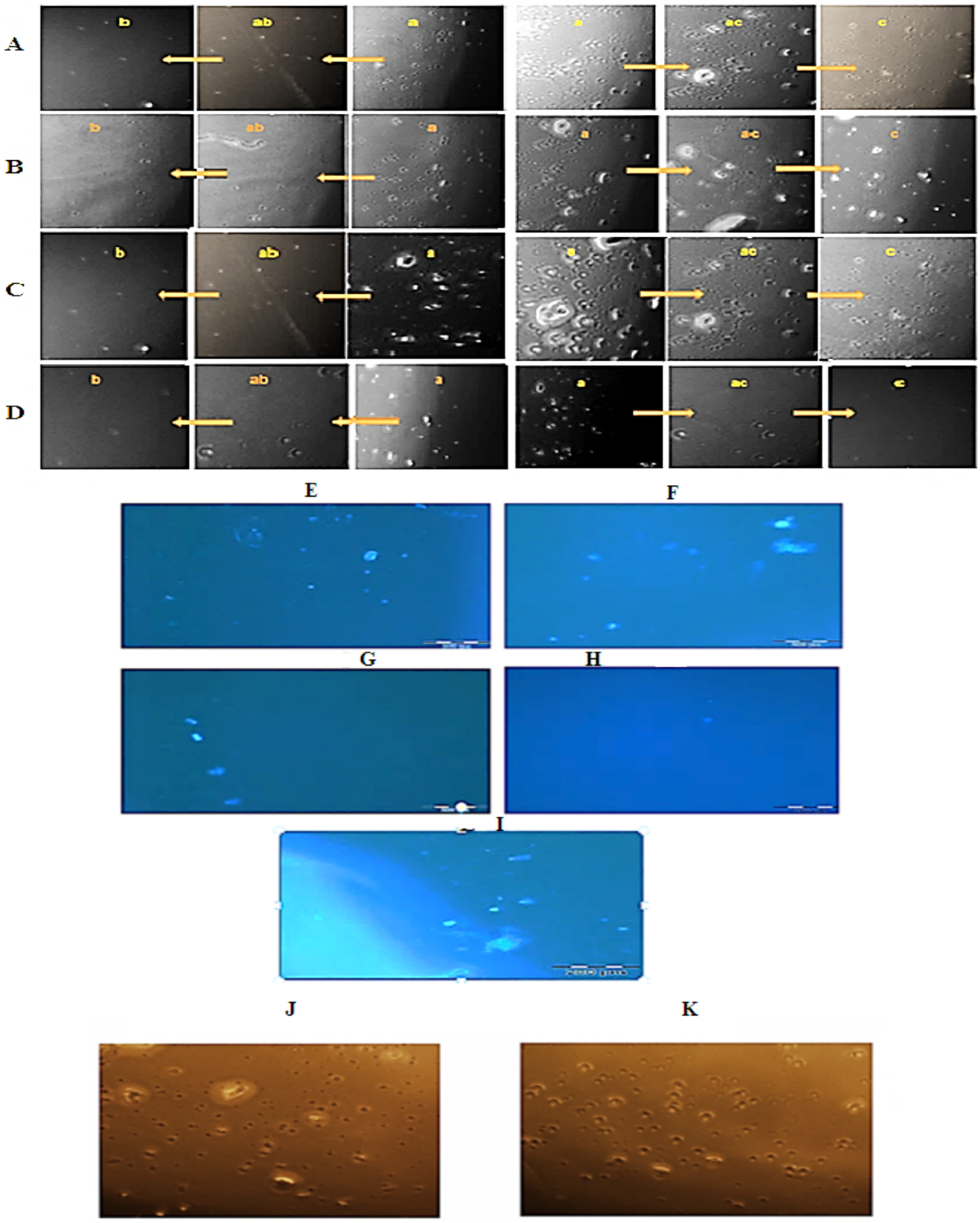
A
B
C
D
E
F
G
H
I
J
K

Figure 7. Migration of PBMC cells in chemotaxis assay. **A to D:** Phase contrast microscope images of chemoattract PBMC cells (cells were seeded in the central well; ab: distance between the well containing cells and the well containing negative control (FBS-free DMEM); ac: distance between the well containing cells and the well containing chemoattractants such as CCL21 or FBS as positive control; c: well containing negative control (FBS-free DMEM); b: well containing chemoattractant (such as CCL21 or FBS) as positive control. **A)** Composite image of cells migrating from cell-containing well to the commercial CCL21 well (right) and the DMEM well (left). **B)** Composite image of cells migrating from cell-containing well to the purified CCL21 well (right) and the non-recombinant protein well (left). **C)** Composite image of cells migrating from cell-containing well to 10% FBS well (right) and DMEM well (left). **D)** Composite image of cells migrating from cell-containing well to the non-recombinant protein well (right) and DMEM well (left). Chemotaxis of each substance was assessed by counting the number of cells migrated to each well. As can be seen, the number of monocyte cells moving toward the absorbent agent is higher than the non-absorbent substance, and chemotaxis of the recombinant protein is estimated to be about 91% (Bar = 200 µm). **E to I:** Nuclear labeling with DAPI staining. A black line represents the interface between agarose wall and the medium. Peripheral blood mononuclear cells (PBMC) migrated after 24 hours of stimulation toward **E)** commercial CCL21, **F)** purified CCL21, **G)** DMEM without 10% FBS, **H)** non-recombinant protein, and **I)** 10% FBS sources. **J&K:** Comparison of cell migration toward recombinant CCL21 protein as chemokinesis (CK) and toward growth factor as chemotaxis (CT). **J)** PBMC migration toward CCL21. **K)** PBMC migration toward 10% FBS. As shown, cells exhibited the same migration toward CCL21, the chemokine, and the growth factor (10% FBS), i.e. the adsorbent.